Phys. Status Solidi A **211,** No. 5, 1162–1167 (2014) / **DOI** 10.1002/pssa.201330298

physica status solidi a
www.pss-a.com
applications and materials science

# Growth of Ru–$SiO_2$ underlayer for $Co_{72}Pt_{28}$–$SiO_2$ nanocomposite films

**Rujun Tang**[*,1] **and Pin Ho**[2]

[1] Jiangsu Key Laboratory of Thin Films, School of Physical Science and Technology, Soochow University, Suzhou 215006, P.R. China
[2] Department of Materials Science and Engineering, National University of Singapore, Singapore 117576, Singapore

Received 12 September 2013, revised 27 December 2013, accepted 20 January 2014
Published online 18 February 2014

**Keywords** CoPt, magnetic properties, microstructure, nanocomposite, Ru

[*] Corresponding author: e-mail rjuntang@gmail.com, Phone: +86 512 65224371, Fax: +86 512 65224371

The effects of sputter growth conditions of Ru–$SiO_2$ underlayer (hereafter referred as $Ru_t$ layer) on the microstructure of this layer were studied. The effects of growth conditions of the $Ru_t$ layer on the microstructure and magnetic properties of the $Co_{72}Pt_{28}$–$SiO_2$ top layer were further investigated. Results show that increasing $SiO_2$ content in the $Ru_t$ layer deteriorates slightly the texture of Ru grains in this layer generally. The high-pressure (1.3 Pa) deposition can better protect the texture of Ru than low-pressure (0.4 Pa) deposition with $SiO_2$ addition. Furthermore, high-pressure deposition of $Ru_t$ layer with low $SiO_2$ content produces better texture of $Co_{72}Pt_{28}$ than low pressure. The sizes of Ru grains and $Co_{72}Pt_{28}$ grains decrease with increasing $SiO_2$ content. A high-pressure deposition of $Ru_t$ layer further reduces the grain size of $Co_{72}Pt_{28}$. Both the coercivity and the remanence ratio of $Co_{72}Pt_{28}$ layer decrease when $SiO_2$ content in the $Ru_t$ layer exceeds 10 vol.%. High-pressure deposition of $Ru_t$ layer results in a higher coercivity and remanence ratio of $Co_{72}Pt_{28}$ layer than those with low-pressure depositions. The above results show that the grain size of $Co_{72}Pt_{28}$ can be reduced without sacrificing its magnetic properties at small $SiO_2$ content.



**1 Introduction** In recent years, the urgent need to engineer the magnetic nanostructures at nanoscale level has led to a growing interest in the preparation, investigation and control of the properties of the magnetic nanoparticles and thin films [1]. One of the major challenges in further increasing the areal density of perpendicular magnetic recording media is in reducing the grain size and improving the signal to noise ratio by minimizing transition noise [2]. Efforts have been made to reduce grain size by adding oxide-based materials into the magnetic layer [3] or by depositing the magnetic layer in an argon and oxygen environment [4]. However, too much oxide in the magnetic layer would reduce its magnetic anisotropy, leading to increased thermal instability due to the superparamagnetic effect. An alternative approach is to reduce the grain size of the intermediate layer and hence, the grain size of the magnetic layer. The addition of synthetic nucleation layers [5], RuCr-oxide underlayer [6], NiAl underlayer [7] and Ar-etched Ru underlayer [8, 9] have been reported to be able to decrease the grain size of the magnetic layer to below 6 nm. However, a deteriorated texture or reduction of the nucleation field of the magnetic layer was also observed. Recently, it was reported that doping oxide into the Ru underlayer could reduce the grain size of magnetic layer [10]. The reduction of grain size was based on a large volume fraction of oxide addition into the Ru underlayer, which deteriorated the texture of the latter. The growth conditions of the Ru-oxide underlayer was not reported in detail. Moreover, the texture information of the CoPt layer, which was important for evaluation of the media qualities, was not obtained. A systematic understanding of the effects of growth conditions on the microstructure of the nano-sized Ru grains, and its effects on the growth of CoPt grains was both scientifically interesting and technologically important. In this paper, $SiO_2$ was doped into the Ru intermediate layer to reduce the grain size of the $Co_{72}Pt_{28}$–$SiO_2$ magnetic layer. The effects of sputtering power, pressure and $SiO_2$ volume fraction of Ru–$SiO_2$ underlayer on the microstructure of this layer were studied. The effects of growth conditions of the Ru–$SiO_2$ layer on the microstructure and magnetic properties of $Co_{72}Pt_{28}$–$SiO_2$ layer were further investigated.

**2 Experimental** Granular films of $Co_{72}Pt_{28}$–$SiO_2$(15 nm)/Ru–$SiO_2$(10 nm)/$Ru_b$(bottom Ru, 15 nm)/Ta

(4 nm)/glass were deposited at room temperature by magnetron sputtering. The base pressure of sputtering was lower than $5 \times 10^{-6}$ Pa. The Ta layer and $Ru_b$ layer were deposited at 0.4 Pa. The Ru–$SiO_2$ (hereafter referred to as $Ru_t$) layer was deposited at 0.4 Pa and 1.3 Pa argon pressures respectively. The $Co_{72}Pt_{28}$, Ru, Ta, and $SiO_2$ targets were used for the sputtering. DC and AC sputtering were used for the metal and $SiO_2$ targets respectively. The volume fraction of $SiO_2$ (hereafter refereed as $V_{SiO_2}$), adjusted by changing the sputtering time of $SiO_2$ relative to that of Ru, was varied from 0 to 20% in the $Ru_t$ underlayer. The composition and thickness of the $Co_{72}Pt_{28}$–$SiO_2$ layer were kept constant in all samples. The crystallographic information of the films were investigated using Philips X'Pert X-ray diffractometer (XRD) with Cu $K\alpha_1$ radiation (source wavelength is 1.5406 Å). The microstructures of the films were investigated using JEOL-2010 transmission electron microscope (TEM). Magnetic properties of the media were measured using the vibrating sample magnetometer (VSM, Lakeshore 7407) under maximum applied field of 1.2 T.

## 3 Results and discussion

**3.1 Microstructures of $Ru_t$ layer** Figure 1 show the $Ru_b/Ru_t$ double layer XRD $\theta$–$2\theta$ spectrum with $Ru_t$ layer deposited at different deposition pressure, power and $V_{SiO_2}$. The $Ru_t$ layer was deposited at low pressure (0.4 Pa) and high pressure (1.3 Pa) with powers of low power (15 W) and high power (50 W) respectively. Figure 1(a) shows the different deposition conditions had not changed the lattice constant $c$ of Ru. The exceptions were for films with $Ru_t$ layer deposited at 15 W and 1.3 Pa, which had a larger lattice constant $c$ of Ru than other films. This larger lattice constant indicated that there was out-of-plane tensile strain in the Ru grains. This tensile strain should be due to the reduced surface curvature of the Ru grains grown at low power and high pressure [11, 12].

The XRD $\theta$–$2\theta$ mode of operation scans through reciprocal space in a direction normal to the substrate surface and thus measure the intensity along such a trajectory in $k$-space, while a rocking curve scans through reciprocal space in a direction parallel to the substrate surface [13, 14]. Hence, the integrated intensity of the symmetric film reflections for a highly textured film in the $\theta$–$2\theta$ mode should be proportional to the film volume and inversely proportional to the rocking curve full width at half maximum (FWHM) squared [14, 15]. A compared analysis of the integrated intensity of the $\theta$–$2\theta$ peak and the rocking curve FWHM could give better understanding on the crystal quality of the highly textured film than that of they alone [15]. The integrated intensity of Ru(00.2) ($Ru_b/Ru_t$) $\theta$–$2\theta$ peaks (hereafter referred as $I_{Ru}$) were given as a function of $V_{SiO_2}$ in Fig. 1(b) and (c). The $I_{Ru}$ was obtained by Gauss fitting to the Ru(00.2) peaks with standard errors smaller than 1% of the $I_{Ru}$. The XRD measurement setups were same for all the films. Therefore, the $I_{Ru}$ should be determined by the volume fraction and the texture of Ru in the $Ru_t$ layer [16].

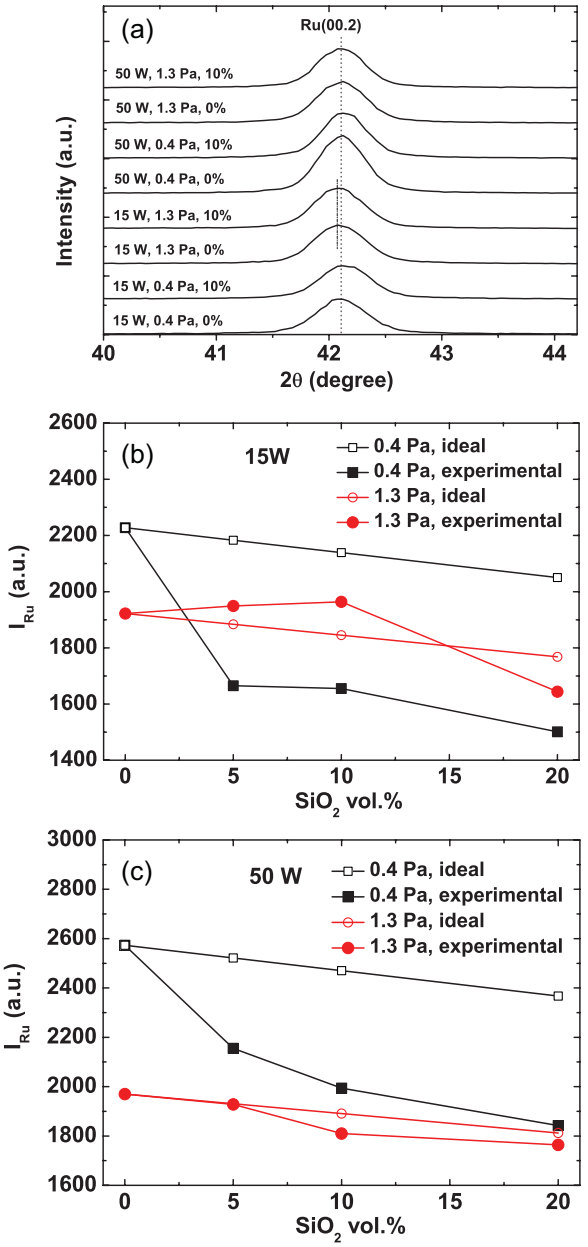


**Figure 1** Plot (a) is the $Ru_b/Ru_t$ double layer XRD $\theta$–$2\theta$ spectrum with $Ru_t$ layer deposited at different deposition pressure, power and $V_{SiO_2}$. Plots (b) and (c) are the integrated intensity of Ru(00.2) ($Ru_b/Ru_t$) $\theta$–$2\theta$ peaks, $I_{Ru}$. The $I_{Ru}$ was obtained by Gauss fitting to the Ru(00.2) peaks with standard errors smaller than 1% of the $I_{Ru}$. The lines were only used to guide the readers' eyes.

The total volume of the Ru and the $SiO_2$ in the $Ru_t$ layer was kept constant during the experiments. We define an "ideal" case that the addition of $SiO_2$ into $Ru_t$ layer only reduces the volume of Ru without changing the texture of Ru. Therefore, in the "ideal" case, $I_{Ru}$ would decrease lineary with increasing $V_{SiO_2}$, as shown in Fig. 1(b) and (c). A deterioration in the texture of Ru would result in a smaller $I_{Ru}$ than the "ideal" case, and vice versa [15]. Figure 1(b) and (c) shows generally, the experimental $I_{Ru}$ reduced with

increasing $V_{SiO_2}$, and the experimental $I_{Ru}$ were smaller than the "ideal" case. The exception was for the 15 W and 1.3 Pa depositions, where experimental $I_{Ru}$ were slightly larger than the "ideal" case when $V_{SiO_2}$ was small. Figure 2 shows the Ru(00.2) XRD rocking curves and the FWHM of the Ru(00.2) rocking curves a function of $V_{SiO_2}$. Figure 2(b) shows the $SiO_2$ addition led generally to an increase in FWHM. The exception was for the 15 W and 1.3 Pa depositions where FWHM decreased slightly when $V_{SiO_2}$ was small. The results in Figs. 1 and 2 agreed qualitatively with each other, indicating a deterioration of the texture of Ru in the $Ru_t$ layer. However, a low power and high-pressure deposition of $Ru_t$ layer might improve the texture of Ru at small $V_{SiO_2}$ instead. The improvement of the texture in this case might be contributed by the local tensile strain in the Ru grains as shown in Fig. 1(a).

Figure 1(b) and (c) also shows for a specific $V_{SiO_2}$, the combination of deposition power and deposition pressure affected the $I_{Ru}$ greatly. The 0.4 Pa deposited Ru had larger $I_{Ru}$ than that at 1.3 Pa depositions without $SiO_2$ addition, indicating a better texture at 0.4 Pa depositions. However, results changed with $SiO_2$ addition. For $Ru_t$ deposited at 15 W, all the $I_{Ru}$ at 0.4 Pa depositions were much smaller than the "ideal" values, while $I_{Ru}$ at 1.3 Pa deposition were larger than the "ideal" values at small $V_{SiO_2}$. For $Ru_t$ deposited at 50 W, all the $I_{Ru}$ at 0.4 Pa depositions were much smaller than the "ideal" values, while $I_{Ru}$ at 1.3 Pa deposition were only slightly smaller than the "ideal" values. The above results agreed qualitatively with the results in Fig. 2(b) where FWHM at 0.4 Pa depositions increased faster than that at 1.3 Pa depositions. These results indicated that in the case of $SiO_2$ addition, 1.3 Pa deposition of the $Ru_t$ layer can better protect the texture of Ru than 0.4 Pa deposition. The total volume of the $Ru_t$ layer was contributed by three components: the volume of Ru, the volume of $SiO_2$, and the volume of void grain boundaries. It was known that Ru film

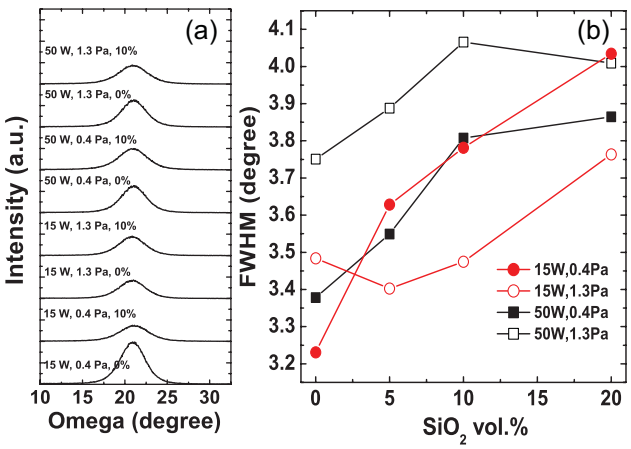


**Figure 2** Plot (a) and (b) are the Ru(00.2) XRD rocking curves and the full width-at-half maximum (FWHM) of the Ru(00.2) rocking curves with $Ru_t$ layer deposited at different deposition pressure, power and $V_{SiO_2}$. The lines were only used to guide the readers' eyes.

tended to form a porous structure with void grain boundaries at high-pressure oblique depositions, while the low-pressure deposition tended to form a denser Ru film due to larger kinetic energy of the Ru adatoms [17]. As a result, the low-pressure deposition could produce a better texture of Ru than high-pressure deposition without $SiO_2$ addition, as shown in Figs 1(b), (c) and 2. However, the void grain boundaries could accommodate some of the $SiO_2$ added in the $Ru_t$ layer. Therefore, the high-pressure deposition can better protect the texture of Ru than low-pressure deposition for a specific $V_{SiO_2}$.

Figure 3 shows the bright field TEM images of $Ru_t$ layer deposited with different $SiO_2$ volume fractions under different pressures. The deposition power of $Ru_t$ was chosen as 50 W because the high power deposition can better protect the texture of Ru at large $V_{SiO_2}$ as shown in Fig. 2. The average and standard deviations of the grain sizes were obtained by log–normal fitting to the grain size data (counted over randomly selected 100 pairs of grains). Figure 3(a) shows for film deposited at 0.4 Pa without $SiO_2$ addition, the Ru grain size was very large and grain boundaries were ill defined. This was due to the high mobility of Ru adatoms at 0.4 Pa deposition. With addition of $SiO_2$, isolated Ru grains were observed. The grain boundaries were deduced to be $SiO_2$ due to the phase separation between Ru and $SiO_2$. For films deposited at 1.3 Pa, isolated grains were observed even without $SiO_2$ addition as shown in Fig. 3(d). This was caused by the low mobility of Ru atoms and the "shadowing effect" [17] of Ru grains at 1.3 Pa deposition.

The grain boundaries were deduced to be voids. This showed that previous explanations on the deposition pressure dependent texture of Ru in Figs. 1 and 2 were justified. With the addition of $SiO_2$, these grain boundaries became a hybrid of voids and oxides. For both deposition pressures, the average grain size decreased with the increase of $SiO_2$ content. However, the grain size distributions increase with the $SiO_2$ content. In addition, the grain size of Ru deposited at 1.3 Pa was slightly smaller than those deposited at 0.4 Pa at the same $SiO_2$ addition.

### 3.2 Microstructures and magnetic properties of $Co_{72}Pt_{28}$–$SiO_2$ layer

The growth conditions of the $Ru_t$ layer on the microstructure and magnetic properties of $Co_{72}Pt_{28}$–$SiO_2$ layer were further investigated. Figure 4(a) shows the combined XRD $\theta$–$2\theta$ peaks of Ru(00.2)-$+Co_{72}Pt_{28}$(00.2) with $Ru_t$ layer deposited at 0.4 and 1.3 Pa, and with different $SiO_2$ additions. The deposition power of $Ru_t$ was 50 W. Figure 4(a) shows the peaks of Ru and $Co_{72}Pt_{28}$ were heavily overlapped due to the very close lattice constant $c$ between $Co_{72}Pt_{28}$(00.2) and Ru(00.2). As a result, the texture information of the $Co_{72}Pt_{28}$ layer could not be determined directly from the XRD results. However, the changes in the integrated intensity of $Co_{72}Pt_{28}$(00.2) (hereafter referred as $I_{CoPt}$) would be mainly determined by the changes in the texture of $Co_{72}Pt_{28}$. This was due to the growth conditions of the $Co_{72}Pt_{28}$ layer were kept same during the experiments. Only the growth conditions of

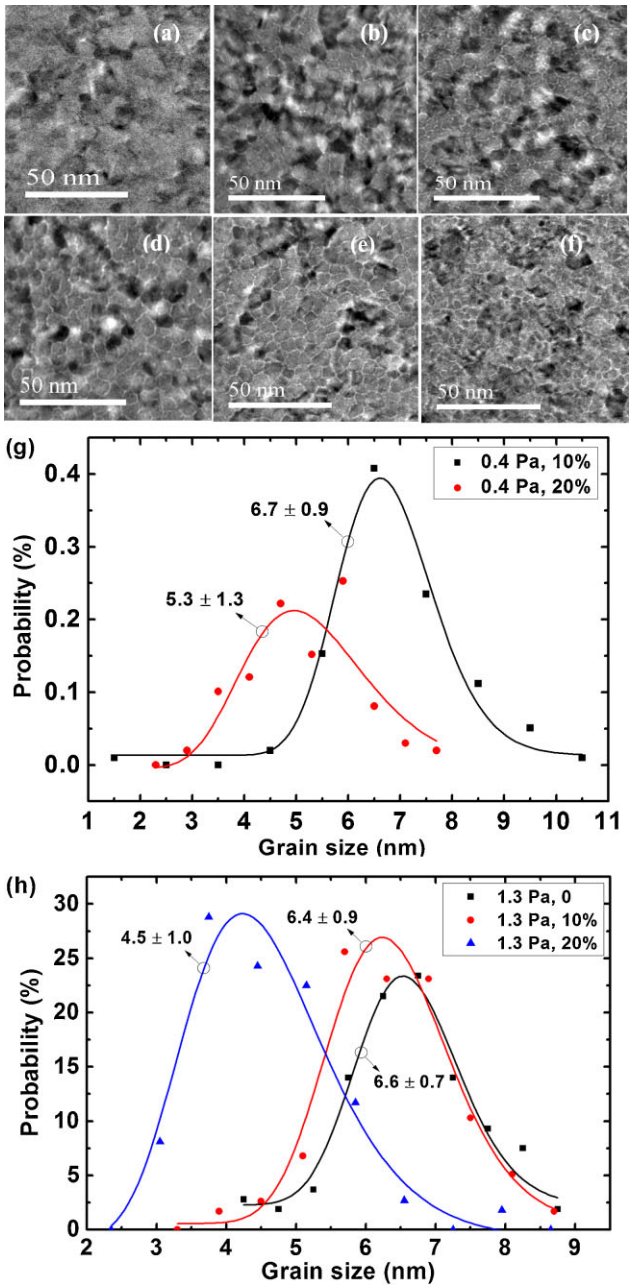


**Figure 3** Planar-view TEM bright field images of $Ru_t$ layer deposited with the $SiO_2$ content and pressure of (a) 0% and 0.4 Pa, (b) 10% and 0.4 Pa, (c) 20% and 0.4 Pa, (d) 0% and 1.3 Pa, (e) 10% and 1.3 Pa, and (f) 20% and 1.3 Pa. The deposition power of $Ru_t$ layer was 50 W. Plots (g) and (h) are the corresponding grain size distributions. The grain size was center to center distance of two neighboring grains. TEM images in this figure were obtained from samples deposited on the carbon coated Cu grids.

the $Ru_t$ underlayer were varied. Therefore, the changes in the texture of $Co_{72}Pt_{28}$ could be estimated from the $I_{CoPt}$. The $I_{CoPt}$ in this paper was obtained by subtracting the integrated intensity of Ru(00.2) $I_{Ru}$ from that of the corresponding combined peaks Ru(00.2) + $Co_{72}Pt_{28}$(00.2) (hereafter referred as $I_{Ru+CoPt}$). The $I_{Ru+CoPt}$ was obtained by Gauss

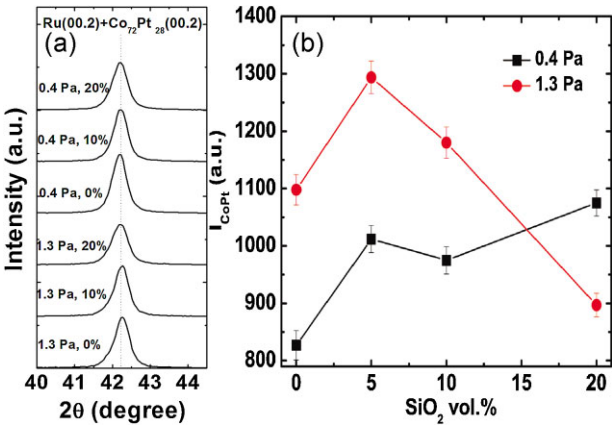


**Figure 4** Plot (a) is combined XRD $\theta$–$2\theta$ peaks of Ru(00.2)-+$Co_{72}Pt_{28}$(00.2) with $Ru_t$ layer deposited at 0.4 and 1.3 Pa, and with different $SiO_2$ additions. The deposition power of $Ru_t$ layer was 50 W. Plot (b) is the integrated intensities of $Co_{72}Pt_{28}$(00.2) peaks $I_{CoPt}$, which were obtained by subtracting the integrated intensities of Ru(00.2) $I_{Ru}$ from those of the combined peaks Ru(00.2) + $Co_{72}Pt_{28}$(00.2) ($I_{Ru+CoPt}$). The error bars in the figure represented the standard errors of $I_{CoPt}$. The lines were only used to guide the readers' eyes.

fitting to the combined peaks Ru(00.2) + $Co_{72}Pt_{28}$(00.2) peaks with standard errors smaller than 1% of the $I_{Ru+CoPt}$. Figure 4(b) shows the $I_{CoPt}$ as a function of $SiO_2$ content in $Ru_t$ layer. From Fig. 4(b), adding 5 vol.% of $SiO_2$ led to a slight increase in $I_{CoPt}$ and hence, an improved texture of $Co_{72}Pt_{28}$ at both 0.4 and 1.3 Pa depositions. With a further increase in $SiO_2$ content beyond 5 vol.%, the $I_{CoPt}$ decreased for $Ru_t$ deposited at 1.3 Pa, whereas there was no notable change in $I_{CoPt}$ for $Ru_t$ deposited at 0.4 Pa. On the other hand, the $I_{CoPt}$ with $Ru_t$ deposited at 1.3 Pa was much higher than that deposited at 0.4 Pa until $SiO_2$ content was 20 vol.%. This suggested that for a small amount of $SiO_2$ addition, 1.3 Pa deposition of $Ru_t$ produced better texture of $Co_{72}Pt_{28}$ than that of 0.4 Pa deposition. This difference should be attributed to the difference in the grain structure of $Ru_t$ because the texture of $Ru_t$ at 0.4 Pa was better than that at 1.3 Pa, as shown in Fig. 2(b). However, more works are needed to understand this phenomenon.

Figure 5 shows the bright field TEM images and grain size distributions of $Co_{72}Pt_{28}$–$SiO_2$ nanocomposite films, with $Ru_t$ deposited at 0.4 Pa (Fig. 5(a)–(c), (g) and (i)) and 1.3 Pa (Fig. 5(d)–(f), (h), and (j)). The deposition power of $Ru_t$ layer was 50 W. The average and standard deviations of the grain sizes were obtained by log-normal fitting to the grain size data (counted over randomly selected 100 pairs of grains). Addition of $SiO_2$ into the $Ru_t$ layer decreased both the grain size and size distribution of $Co_{72}Pt_{28}$ grains for 0.4 Pa deposited $Ru_t$ layer. The reduction of $Co_{72}Pt_{28}$ grain size and size distribution was also observed for 1.3 Pa deposited $Ru_t$ layer with vol.5% $SiO_2$. Further increasing $SiO_2$ content to vol.10% did not lead to a further reduction in the grain size for 1.3 Pa deposition. The reduction of grain size was attributed to the smaller Ru grains and the enhanced

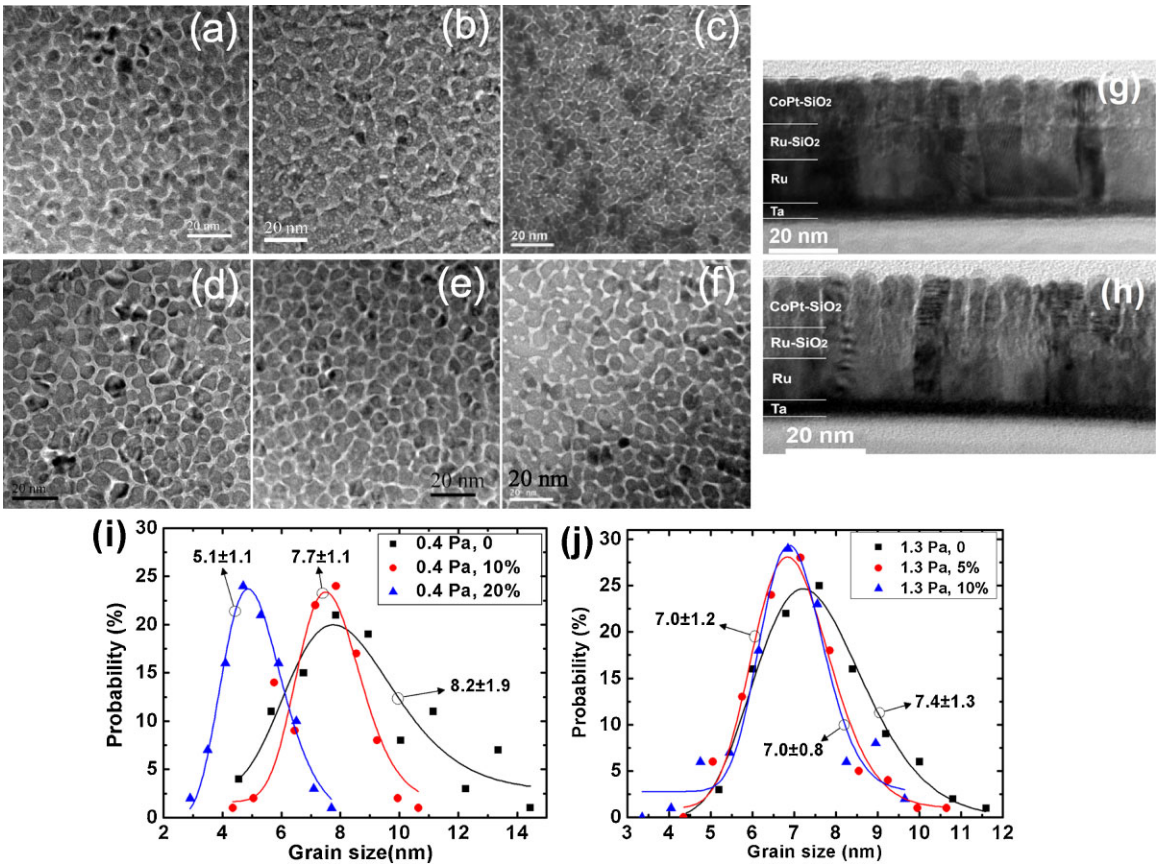


**Figure 5** TEM bright field images of $Co_{72}Pt_{28}$–$SiO_2$ nanocomposite films with $Ru_t$ deposited under different conditions. Images (a), (b), and (c) are the planar-view images with $Ru_t$ deposited at 0.4 Pa with $Ru_t$ layer $SiO_2$ content of 0%, 10 vol.% and 20 vol.%, respectively. Images (d), (e), and (f) are the planar-view images with $Ru_t$ deposited at 1.3 Pa with $Ru_t$ layer $SiO_2$ content of 0%, 5 vol.% and 10 vol.%, respectively. Images (g) and (h) are cross-section images of the samples in (b) and (f). Plot (i) and (j) are grain size distributions of $Co_{72}Pt_{28}$ with $Ru_t$ deposited at 0.4 and 1.3 Pa and various $SiO_2$ content. The grain size was center to center distance of two neighboring grains.

oxide segregation in the initial growth region of the $Co_{72}Pt_{28}$ layer [18]. The average grain size of $Co_{72}Pt_{28}$ layer with $Ru_t$ layer deposited at 1.3 Pa was smaller than that at 0.4 Pa when $SiO_2$ content was smaller than 20 vol.%. This was due to the better isolated Ru grains in the $Ru_t$ layer deposited at 1.3 Pa than at 0.4 Pa, as shown in Figs. 3 and 5(g) and (h).

Figure 6 shows the dependence of out-of-plane hysteresis loops, coercivities ($H_c$) and remanence ratios ($m_R = M/M_S$) of $Co_{72}Pt_{28}$–$SiO_2$ nanocomposite films with $Ru_t$ deposited at 0.4 and 1.3 Pa and various $SiO_2$ additions. For $Co_{72}Pt_{28}$ film with $Ru_t$ deposited at 1.3 Pa, adding 5 vol. % $SiO_2$ into the $Ru_t$ did not lead to noticeable changes in $H_c$. With further increasing in $SiO_2$ content, the $H_c$ decreased. For $Co_{72}Pt_{28}$ film deposited at 0.4 Pa, adding $SiO_2$ into the $Ru_t$ did not lead to appreciable changes in $H_c$. There was no notable change in $m_R$ of the film until $SiO_2$ content was 20 vol.% for both 0.4 and 1.3 Pa deposition. When $SiO_2$ content was 20 vol.%, $m_R$ reduced. The reduction of $m_R$ could be attributed to both deteriorated texture and reduced grain size which increased the thermal demagnetization of the film. On the other hand, the $Co_{72}Pt_{28}$–$SiO_2$ film with $Ru_t$ deposited at 1.3 Pa displayed both higher $H_c$ and $m_R$ than those with $Ru_t$ deposited at 0.4 Pa. The $H_c$ of the film was determined by both the microstructure of the $Co_{72}Pt_{28}$ grains and magnetization reversal mechanism of the film. Therefore, the higher $H_c$ and $m_R$ at 1.3 Pa were possibly attributed to the better texture of $Co_{72}Pt_{28}$ at 1.3 Pa than that at 0.4 Pa as shown in Fig. 4.

**4 Summary** In this paper, the effects of sputter growth conditions of $Ru_t$ underlayer on the microstructure of this layer were studied. The effects of growth conditions of the $Ru_t$ layer on the microstructure and magnetic properties of $Co_{72}Pt_{28}$–$SiO_2$ top layer were further investigated. Results showed that both the $SiO_2$ content and the deposition conditions (pressure and power) affected the Ru underlayer texture greatly. Increasing $SiO_2$ content in the $Ru_t$ layer deteriorated slightly the texture of Ru grains in this layer generally. Although the low-pressure (0.4 Pa) deposition could produce a better texture of Ru than high-pressure (1.3 Pa) deposition without $SiO_2$ addition, high-pressure deposition could better protect the texture of Ru than low-pressure deposition with $SiO_2$ addition. Furthermore, the high-pressure deposition of $Ru_t$ layer at low $SiO_2$ content

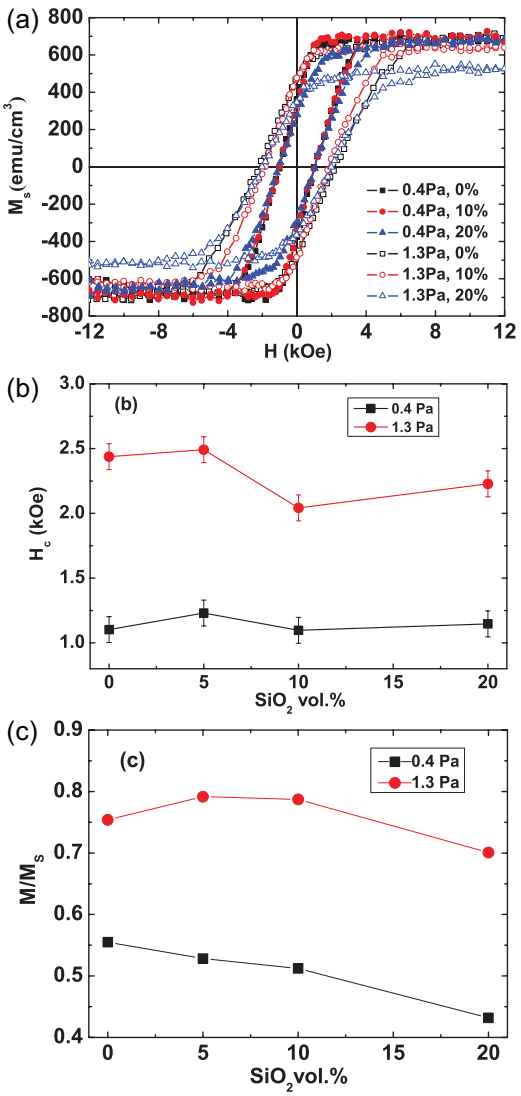


**Figure 6** Plot (a) was the out-of-plane hysteresis loops of $Co_{72}Pt_{28}$–$SiO_2$ nanocomposite films $Ru_t$ deposited at 0.4 Pa and 1.3 Pa and various $SiO_2$ additions (0%, 10 vol.% and 20 vol.%). The deposition power of $Ru_t$ layer was 50 W. Plots (b) and (c) are coercivity and remanence ratio of the films as a function of $V_{SiO_2}$ in the $Ru_t$. The error bars represented the standard error of the mean. The lines were only used to guide the readers' eyes.

produced better texture of $Co_{72}Pt_{28}$ grains grown on it than low pressure. The sizes of the Ru grains and $Co_{72}Pt_{28}$ grains decreased from $6.7 \pm 0.9$ to $5.3 \pm 1.3$ nm and from $8.2 \pm 1.9$ to $5.1 \pm 1.1$ nm with the addition of $SiO_2$ up to 20 vol.%, respectively. A high-pressure deposition of $Ru_t$ layer further reduced the grain size of $Co_{72}Pt_{28}$ due to the porosity in the grain boundary regions of the $Ru_t$ layer. Adding 5 vol.% $SiO_2$ into the $Ru_t$ did not lead to noticeable changes in the coercivity and remanence ratio of the $Co_{72}Pt_{28}$ layer. Further increasing $SiO_2$ content in $Ru_t$ layer led to the decrease of both the coercivity and the remanence ratio of $Co_{72}Pt_{28}$ layer. A high-pressure deposition of $Ru_t$ layer resulted in a higher coercivity and remanence ratio of the $Co_{72}Pt_{28}$ layer than those with low-pressure depositions. The above results suggested that the high-pressure deposition with a small amount of $SiO_2$ addition could reduce the grain size of the $Ru_t$ layer and hence, the $Co_{72}Pt_{28}$ layer without adversely affecting the magnetic properties of the $Co_{72}Pt_{28}$ layer.

**Acknowledgements** The authors thank the technical support from Prof. Chow Gan-Moog and Assistant Prof. Dr. Chen Jingsheng, as well as helpful discussions with Dr. Pandey Koashal Kishor Mani from the National University of Singapore (NUS) and Dr. Hu Jiangfeng from the Data Storage Institute in Singapore. The author R.J. Tang thanks the support of Scholarship from the China Scholarship Council. This work is partially supported by the Agency for Science, Technology and Research (A*STAR) Singapore under Grant No. 062-101-0021, and FRC of NUS under Grant No. R-284-000-053-112.

## References

[1] S. D. Bader, Rev. Mod. Phys. **78**, 1 (2006).
[2] S. Iwasaki, IEEE Trans. Magn. **20**, 657 (1984).
[3] M. Zheng, B. R. Acharya, G. Choe, J. N. Zhou, Z. D. Yang, E. N. Abarra, and K. E. Johnson, IEEE Trans. Magn. **40**, 2498 (2004).
[4] Y. Inaba, T. Shimatsu, T. Oikawa, H. Sato, H. Aoi, H. Muraoka, and Y. Nakamura, IEEE Trans. Magn. **40**, 2486 (2004).
[5] S. N. Piramanayagam, C. K. Pock, L. Li, C. Y. Ong, C. S. Mah, and J. Z. Shi, Appl. Phys. Lett. **89**, 162504 (2006).
[6] S. N. Piramanayagam, J. Z. Shi, H. B. Zhao, C. K. Pock, C. S. Mah, C. Y. Ong, J. M. Zhao, J. Zhang, Y. S. Kay, and L. Lu, IEEE Trans. Magn. **43**, 633 (2007).
[7] H. Yuan, Y. L. Qin, and D. E. Laughlin, Thin Solid Films **517**, 990 (2008).
[8] H. Yuan and D. E. Laughlin, Appl. Phys. Lett. **93**, 102511 (2008).
[9] H. Yuan and D. E. Laughlin, J. Appl. Phys. **105**, 07B707 (2009).
[10] H. Yuan, D. E. Laughlin, X. Zhu, and B. Lu, J. Appl. Phys. **103**, 07F513 (2008).
[11] K. K. M. Pandey, J. S. Chen, B. C. Lim, and G. M. Chow, J. Appl. Phys. **104**, 073904 (2008).
[12] S. Yonemura, S. Saito, A. Hashimoto, and M. Takahashi, J. Magn. Magn. Mater. **320**, 3053 (2008).
[13] B. D. Cullity, Elements of X-Ray Diffraction, second ed. (Addison-Wesley Publ. Co., Inc., Reading, Massachusetts, 1978), p. 488.
[14] G. Bauer and W. Richter, Optical Characterization of Epitaxial Semiconductor Layers, first ed. (Springer, Berlin, 1996), p. 289.
[15] E. McCarthy, R. T. Rajendra Kumar, B. Dogget, S. Chakrabarti, R. J. O'Haire, S. B. Newcomb, J.-P. Mosnier, M. O. Henry, and E. McGlynn, J. Phys. D: Appl. Phys. **44**, 375401 (2011).
[16] M. D. Vaudin, J. Res. Natl. Inst. Stand. Technol. **106**, 1063 (2001).
[17] J. A. Thornton, J. Vac. Sci. Technol. A **4**, 3095 (1986).
[18] I. Takekuma, R. Araki, M. Igarashi, H. Nemoto, I. Tamai, Y. Hirayama, and Y. Hosoe, J. Appl. Phys. **99**, 08E713 (02006).